Plasma Chem Plasma Process (2016) 36:85–105
DOI 10.1007/s11090-015-9657-2

REVIEW ARTICLE

Plasma Assisted Low Temperature Combustion

Yiguang Ju[1] · Joseph K. Lefkowitz[1] · Christopher B. Reuter[1] · Sang Hee Won[1] · Xueliang Yang[1] · Suo Yang[2] · Wenting Sun[2] · Zonglin Jiang[3] · Qi Chen[4]

Received: 30 June 2015 / Accepted: 1 September 2015 / Published online: 1 October 2015

Abstract This paper presents recent kinetic and flame studies in plasma assisted low temperature combustion. First, the kinetic pathways of plasma chemistry to enhance low temperature fuel oxidation are discussed. The impacts of plasma chemistry on fuel oxidation pathways at low temperature conditions, substantially enhancing ignition and flame stabilization, are analyzed base on the ignition and extinction *S*-curve. Secondly, plasma assisted low temperature ignition, direct ignition to flame transition, diffusion cool flames, and premixed cool flames are demonstrated experimentally by using dimethyl ether and n-heptane as fuels. The results show that non-equilibrium plasma is an effective way to accelerate low temperature ignition and fuel oxidation, thus enabling the establishment of stable cool flames at atmospheric pressure. Finally, the experiments from both a non-equilibrium plasma reactor and a photolysis reactor are discussed, in which the direct measurements of intermediate species during the low temperature oxidations of methane/methanol and ethylene are performed, allowing the investigation of modified kinetic pathways by plasma-combustion chemistry interactions. Finally, the validity of kinetic mechanisms for plasma assisted low temperature combustion is investigated. Technical challenges for future research in plasma assisted low temperature combustion are then summarized.

Keywords Plasma assisted combustion · Low temperature chemistry · Kinetics · Cool flames

✉ Yiguang Ju
yju@princeton.edu

[1] Department of Mechanical and Aerospace Engineering, Princeton University, Princeton, NJ 08544, USA

[2] Department of Aerospace Engineering, Georgia Institute of Technology, Atlanta, GA 30332, USA

[3] Institute of Mechanics, Chinese Academy of Sciences, Beijing 100190, China

[4] Department of Power and Energy Engineering, Beijing Jiaotong University, Beijing 100044, China

Introduction

Plasma provides a promising solution to control ignition and flame stabilization in engines and high speed propulsion systems [1–3]. As shown schematically in Fig. 1 [1], there are four major plasma assisted combustion enhancement pathways, the thermal effect via temperature rise, the kinetic effect via plasma generated electronically and vibrationally excited molecules and active radicals, the diffusion transport enhancement effect via fuel decomposition and low temperature oxidation, and the convective transport enhancement due to plasma generated ionic wind, hydrodynamic instability, and flow motion via Coulomb and Lorentz forces. The thermal enhancement effect on combustion is through the sensitivity of reaction rates to temperature via the Arrhenius law, which is well understood in flame extinction experiments [4]. The diffusion transport enhancement effect on combustion due to fuel dissociation and fragmentation is also understood through the analysis of flame kernel development and minimum ignition energy [5]. In this effect, small fuel molecules such as H_2, CH_4, CH_2O, and C_2H_4 are created by plasma discharge from the decomposition of large molecule parent fuels. These small fuel molecules diffuse faster into the reaction zone and thus increase flame speed and reduce ignition energy in a stretched flow field [6]. The convective transport enhancement of combustion due to plasma instability and ionic wind has also been extensively studied in [7] and [8–10]. However, the kinetic enhancement effects on combustion of plasma-produced ions, radicals, and excited species have not been studied to a large extent, especially at low temperature [1–3, 11–17].

Most previous studies of plasma assisted combustion focused on ignition and flames involving high temperature chemistry (above 1100 K) [1–4, 7, 8, 15–17]. Recently, by using a nano-second discharge in counterflow ignition of methane and dimethyl ether, it was found that plasma can accelerate low temperature ignition so significantly that the conventional ignition to extinction *S*-curve is transferred into a direct ignition to extinction curve without an extinction limit [13, 18]. Moreover, it was shown that non-equilibrium plasma discharge can accelerate the cool flame chemistry and enable the establishment of self-sustained diffusion and premixed cool flames even at atmospheric pressure [19, 20]. A more recent numerical study of the plasma effect on the negative temperature coefficient behavior and multistage ignition of propane-air mixtures [21] also showed that plasma can

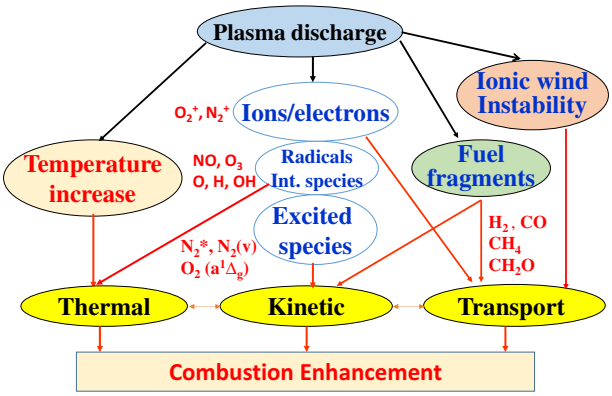

Fig. 1 Major combustion enhancement pathways of plasma assisted combustion [1]

accelerate cool flame ignition. However, many of the kinetic mechanisms governing plasma assisted low temperature chemistry are poorly understood [22].

In this paper, we will present the recent results of plasma assisted low temperature combustion from Princeton University and discuss kinetic pathways of plasma assisted low temperature fuel oxidation.

Results and Discussions

Kinetic Enhancement Pathways of Plasma Assisted Low Temperature Combustion

Large molecule hydrocarbon and oxygenated fuels such as gasoline, diesel, jet fuels, and biodiesel are widely used in transportation and often have rich reactivity at low and intermediate temperatures (Fig. 2). Control of low temperature ignition is very important to achieve higher efficiency and low emissions in advanced engines. A schematic of the temperature-dependent fuel oxidation pathways of a hydrocarbon fuel (RH) with plasma discharge is shown in Fig. 2.

At low temperature (below 700 K), fuel oxidation starts with H-abstraction from the fuel by a radical (e.g. OH) and forms a fuel radical (R). Then, the fuel radicals (R) react with oxygen molecules (O_2) to form RO_2. The internal isomerization of RO_2 will then lead to QOOH (hydroperoxy alkyl radical). After that, a second oxygen addition to QOOH forms O_2QOOH. The subsequent isomerization and decomposition of O_2QOOH will eventually produce two OH radicals. Therefore, this oxidation pathway is the major chain-branching process for low temperature fuel oxidation, which can be summarized as following [23],

$$\mathrm{RH} + \mathrm{X} \rightarrow \mathrm{R} + \mathrm{HX}, \quad \mathrm{X} = \mathrm{H}, \mathrm{OH}, \mathrm{O}, \mathrm{HO_2}, \mathrm{CH_3} \ldots \tag{R1}$$

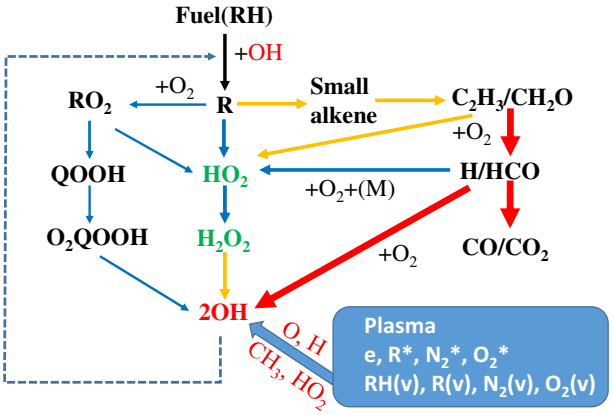

Fig. 2 A schematic of the key reaction pathways for plasma assisted fuel oxidation at different temperatures (*blue arrow* below 700 K; *yellow arrow* 700–1050 K; *red arrow* above 1050 K). Note that those critical temperature conditions are pressure dependent. e: energetic electrons, *: electronically excited or ionized molecules; v: vibrationally excited molecules (Color figure online)

$$R + O_2 \leftrightarrow RO_2 \quad (R2)$$

$$RO_2 \leftrightarrow QOOH \quad (R3)$$

$$QOOH \rightarrow \text{cyclic ether} + OH \quad (R4)$$

$$QOOH + O_2 \leftrightarrow O_2QOOH \quad (R5)$$

$$O_2QOOH \rightarrow RCO + CH_2O + 2OH \quad (R6)$$

The rate limiting reactions in the above reaction pathways are R1 and R3. Since at low temperature the radical concentrations (e.g. OH and HO_2) are very low, the above low temperature fuel oxidation pathway is very slow and normally is too slow to be observed at atmospheric pressure.

At intermediate temperature (700–1050 K), the fuel radicals will thermally decompose into small olefins (e.g. C_2H_4), H atom or alkyl radicals (e.g. CH_3, C_2H_5). After that, CH_2O and C_2H_3 are oxidized to form HCO, HO_2, and H_2O_2 and release heat. As the temperature increases, H_2O_2 decomposes and forms two OH radicals. Therefore, this process is the major chain branching reaction pathway at intermediate temperature and can be summarized as following:

$$C_2H_3 + O_2 \rightarrow C_2H_2 + HO_2 \quad (R7text-1)$$

$$C_2H_3 + O_2 \rightarrow CH_2O + HCO \quad (R7text-2)$$

$$CH_2O + X \rightarrow HCO + XH \quad (R8)$$

$$HCO + O_2 \rightarrow HO_2 + CO \quad (R9)$$

$$HCO + (M) \rightarrow H + CO \quad (R10)$$

$$H + O_2 + (M) \rightarrow HO_2 + (M) \quad (R12)$$

$$HO_2 + HO_2 \rightarrow H_2O_2 + O_2 \quad (R13)$$

$$H_2O_2 \rightarrow OH + OH \quad (R14)$$

The rate limiting reaction in above reaction pathways is R14. Note that although the above reaction pathway at intermediate temperature is faster than the low temperature reaction pathway, it is very sensitive to temperature and limited by the low radical (X) concentration.

At high temperature (above 1050 K), HCO will decompose directly to H and CO and the subsequent hydrogen reaction pathway will produce two or more OH radicals. This high temperature chain-branching reaction pathways can be summarized as:

$$HCO + (M) \rightarrow H + CO + (M) \quad (R10)$$

$$H + O_2 \rightarrow OH + O \quad (R15)$$

$$O + H_2 \rightarrow OH + H \quad (R16)$$

Note that the above high temperature reaction pathway is limited by R15, which is strongly temperature dependent.

With a non-equilibrium plasma discharge, the direct electron impact dissociation reaction processes and the subsequent energy transfer processes between electronically excited species, vibrationally excited species, intermediate species, and reactants provides

new pathways to generate active radicals. Several key radical production pathways by non-equilibrium plasma can be summarized as following [1–3]:

$$e + RH \rightarrow R^* + H + e \quad \text{(R17)}$$

$$e + O_2 \rightarrow O + O(^1D) + e \quad \text{(R18)}$$

$$e + O_2^+ \rightarrow O + O \quad \text{(R19)}$$

$$N^+ + O_2 \rightarrow O^+ + NO \quad \text{(R20)}$$

$$H + O_2(^1\Delta_g) \rightarrow O + OH \quad \text{(R21)}$$

$$O(^1D) + RH \rightarrow OH + R \quad \text{(R22a)}$$

$$N_2(A, B, C) + O_2 \rightarrow O + O + N_2 \quad \text{(R23)}$$

$$N_2(v) + O_2 \rightarrow O + O + N_2 \quad \text{(R24a)}$$

$$N_2(v) + HO_2 \rightarrow OH + O + N_2 \quad \text{(R24b)}$$

$$R^* + O_2 \leftrightarrow RO_2 \quad \text{(R25a)}$$

$$R^* + O_2 \leftrightarrow RO + OH \quad \text{(R25b)}$$

$$O_3 + M \rightarrow O + O_2 + M \quad \text{(R26)}$$

Therefore, as shown in Fig. 2, with a non-equilibrium plasma discharge, the low temperature plasma radical production pathway provides a new source of radical production to accelerate and change the combustion kinetics. A recent flux analysis [1] shows that at low and intermediate temperature (below 1050 K), the plasma radical production rate via R18 is much faster than the rate limiting reactions at both low temperature (R3) and intermediate temperature (R14). However, at higher temperature (1200 K above), the rates of plasma radical production pathways are slower than the rate limiting reaction R15. As such, the rate ratio between plasma radical production and combustion chain-branching reactions will significantly affect the extent of the kinetic enhancement effect of plasma assisted combustion at different temperatures and/or ignition stages.

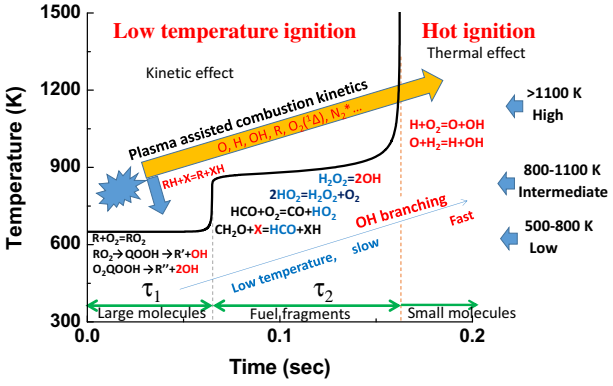

Fig. 3 Schematic of the two-stage ignition of n-heptane, key reaction pathways at low, intermediate, and high temperature ignition (650 K and 20 atm), and the impact of plasma chemistry on the key reaction pathways at different temperatures

For example, for n-heptane ignition at 650 K and 20 atm, there are two ignition stages, the first stage low temperature ignition between 500 and 800 K (τ_1) and the second stage intermediate temperature ignition between 800 and 1100 K (τ_2), as shown in Fig. 3. The 1st and 2nd stages are governed by reactions R3 and R14, respectively. As discussed above, because of the extremely low concentration of radicals (X) in the first stage ignition, R3 is the rate limiting reaction step to produce initial radical (OH) for R1 to generate hydrocarbon radicals (R). As such, radical production via the plasma pathways (R17–R26) will dramatically enhance low temperature combustion. Similarly, during 2nd stage ignition, the rate limiting reaction R14 is also slow to convert unreactive radical HO_2 to much more reactive OH radicals. Therefore, the plasma pathways will also significantly enhance 2nd stage ignition. At higher temperature (1200 K above) or after the 2nd stage ignition, the reactant temperature becomes so high that the chain-branching reaction (R15) is much faster than the reaction rate of the plasma radical production pathway. Therefore, the major role of plasma discharges for high temperature combustion is either to accelerate the chain initiation reactions or to add thermal energy to accelerate reaction R15. From the above discussion, we can conclude that the non-equilibrium plasma can kinetically enhance low temperature combustion more than high temperature combustion.

Since all combustion processes with low temperature chemistry (LTC) are governed by the ignition to extinction *S*-curve [24] (Fig. 4) and because plasma enhances low temperature combustion more than high temperature flames, as shown in Fig. 4, with radical production by non-equilibrium plasma chemistry, the low temperature ignition time can be shortened so much that low temperature combustion can occur at much shorter flow time scales. Moreover, if the plasma intensity (radical production from plasma) is high, the high temperature flame extinction limit will disappear and a direct ignition to flame transition regime without an extinction limit will appear. As such, with plasma discharges one can observe or establish cool flame combustion even at atmospheric pressure in a laboratory burner. In the next section, we will present experimental results of low temperature ignition and cool flame formation at low and atmospheric pressure by using plasma discharges.

Plasma Assisted Low Temperature Ignition and Cool Flames

Plasma Assisted Low Temperature Ignition and Direct Ignition to Flame Transition

We first studied the effect of non-equilibrium plasma activated low temperature chemistry (PA-LTC) on the ignition and extinction of Dimethyl Ether (DME)/O_2/He diffusion flames by using a counterflow burner with in situ nanosecond pulsed discharge at low pressure (72 Torr). As shown in Fig. 5 [18], a uniform nanosecond pulsed discharge is formed

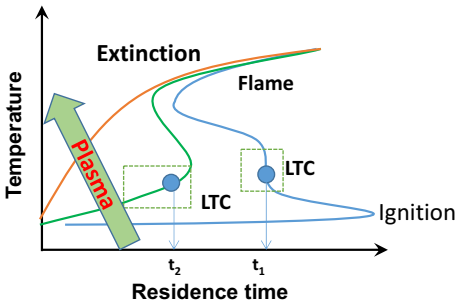

Fig. 4 The dependence of peak flame temperature on the flow residence time: the impact of non-equilibrium plasma discharge on the transition of ignition to extinction *S*-curve with the increase of plasma intensity

between the two counterflow burner nozzles. This is accomplished by placing porous metallic plates, which act both as flow nozzles and electrodes, at the exits of the burner. The separation distance between the two oxidizer and fuel burner nozzles (electrodes) is maintained at 16 mm. The oxidizer-side and fuel-side electrodes are connected to the positive and negative terminals of the high voltage plasma source, respectively, with the same polarization during all experiments. The high voltage pulse is generated by a pulse generator (FID, FPG 30–50MC4) with pulse duration of 12 ns (full width at half maximum, FWHM) and adjustable frequency. The voltage is measured by using a high voltage probe (LeCroy, PPE20KV) and kept constant at 7.6 kV during the experiments. The current through the electrodes is measured by a Pearson Coil (Model 6585). The pulse energy supplied to the discharge is estimated from the time integration of the voltage and current profiles and is approximately 0.73 mJ/pulse. The pulse repetition frequency (f) is fixed at either 24 or 34 kHz during the experiments.

Helium (He) is used as the dilution gas for both the fuel (DME) and the oxidizer (O_2) streams. OH and CH_2O Planar Laser Induced Fluorescence (PLIF) are employed in this study to characterize the high and low temperature chemistry [18]. The OH PLIF intensity is calibrated with a CH_4/O_2/He diffusion flame, so the measured intensity of the PLIF signal can be converted into absolute OH number density. In CH_2O PLIF, formaldehyde is excited by photons at 355 nm with a frequency tripled Nd:YAG laser, and the CH_2O fluorescence signal from the $\tilde{A}^1A_2$ to $\tilde{X}^1A_1$ transition band is collected by an ICCD camera with a bandpass filter between 400 and 450 nm.

CH_2O is a major intermediate species of the low temperature oxidation of DME. The measured CH_2O PLIF signal intensity as a function of fuel mole fraction at the fuel side nozzle exit, X_F, at a plasma repletion rate of $f = 24$ kHz, an oxidizer mole fraction of $X_O = 0.6$, and a flow stretch rate of $a = 250$ 1/s (4 ms flow residence time), is shown in Fig. 6a. It is seen that with an increase in the fuel mole fraction (X_F), the CH_2O PLIF signal intensity increases dramatically. This rapid increase in CH_2O before ignition indicates the occurrence of low temperature DME oxidation. However, when the DME mole fraction is larger than 6 %, high temperature ignition occurs noted by a sharp decrease in the CH_2O concentration. After high temperature ignition the CH_2O PLIF signal intensity becomes insensitive to the increase in fuel mole fraction. On the other hand, when the DME mole fraction is decreased to 5 %, flame extinction occurs with a rapid increase in CH_2O PLIF signal intensity. The hysteresis between ignition and extinction is typical of the ignition–extinction S-curve. As shown previously in Fig. 4, the present results suggests that non-equilibrium plasma can activate low temperature combustion at a much shorter flow time scale of 4 ms at low pressure.

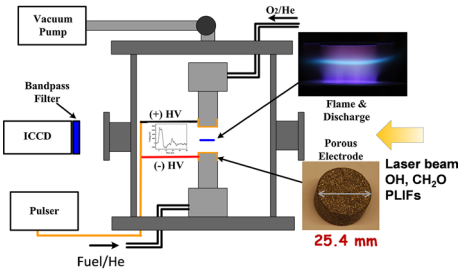

Fig. 5 Schematic of nano-second plasma activated low temperature ignition in a low pressure counterflow flame (72 torr)

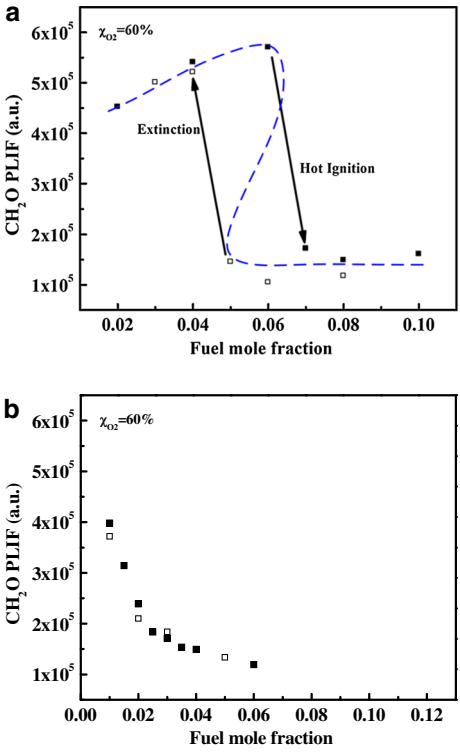

Fig. 6 Relationship between CH_2O PLIF and fuel mole fraction at **a** $X_O = 0.6$, P = 72 Torr, $f = 24$ kHz, and a = 250 1/s, **b** $X_O = 0.6$, P = 72 Torr, $f = 34$ kHz, and a = 250 1/s (*solid square symbols* increasing X_F, *open square symbols* decreasing X_F)

With the increase in the discharge frequency to 34 kHz, Fig. 6b shows that the increase in plasma generated radicals changes the conventional ignition–extinction *S*-curve to a monotonic stretched *S*-curve without hysteresis or an extinction limit. Therefore, non-equilibrium plasma discharges can promote low temperature chemistry and result in a smooth transition between ignition and flame, thus enhancing combustion stability at low temperature.

The kinetic pathway of radical production by non-equilibrium plasma is shown in Fig. 7. It is seen that electron and ion (He^+) collisional dissociation of oxygen is the major

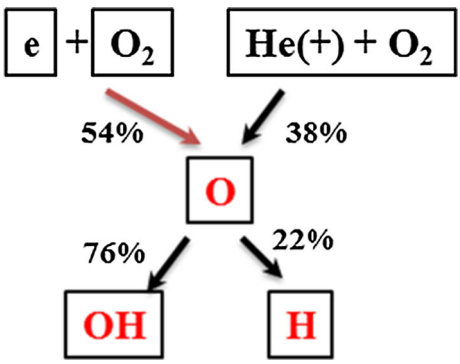

Fig. 7 Path flux analysis: OH and H formation pathways by plasma at $X_F = 0.01$, $X_O = 0.4$, P = 72 Torr, $f = 24$ kHz, and a = 250 1/s

source of O and O(^{1}D) radical production, which leads to the subsequent formation of OH and H to activate the low temperature combustion chemistry of DME oxidation (Fig. 2).

Plasma Assisted Diffusion Cool Flames

To understand further how atomic oxygen production in the plasma discharge can enhance low temperature combustion, experiments were carried out to determine whether a diffusion cool flame can be established using ozone seeding into the oxidizer stream of a counterflow burner [19]. By producing ozone far upstream of the burner exit, the effect of atomic oxygen addition (carried by stable ozone molecules) can be observed independently from other plasma produced species and without any thermal enhancement effects. The experimental geometry (Fig. 8) is similar to the counterflow flame in Fig. 5. However, instead of using direct in situ plasma discharge, ozone is produced by a plasma discharge in a pure oxygen stream at 300 K using a dielectric barrier discharge ozone generator (Ozone Solutions, TG-20). The fuel stream (n-heptane/N_2) is preheated to 550 K. Ozone then decomposes and releases O radicals into the flame preheating zone via reaction R26 to accelerate the low temperature chemistry.

Figure 8 (right) shows direct photos of a cool diffusion flame and a conventional hot diffusion flame at identical flow conditions of 3 % ozone produced in the oxidizer stream, a fuel mole fraction (X_f) of 0.07, and a flow strain rate of $a = 100\ s^{-1}$. With ozone generation from the plasma enhancing the low temperature chemistry (LTC), a self-sustaining cool diffusion flame (Fig. 8b) is successfully established at atmospheric pressure. For the sake of comparison, a hot diffusion flame (the normal high temperature diffusion flame) is shown in Fig. 8a at the same conditions but is initiated by a high temperature torch directly from the existing cool diffusion flame. Comparing between the two shows that the hot diffusion flame has strongly incandescent yellow emission from soot particles due to high temperature fuel pyrolysis, whereas the cool diffusion flame shows very weak bluish chemiluminescence with no soot formation.

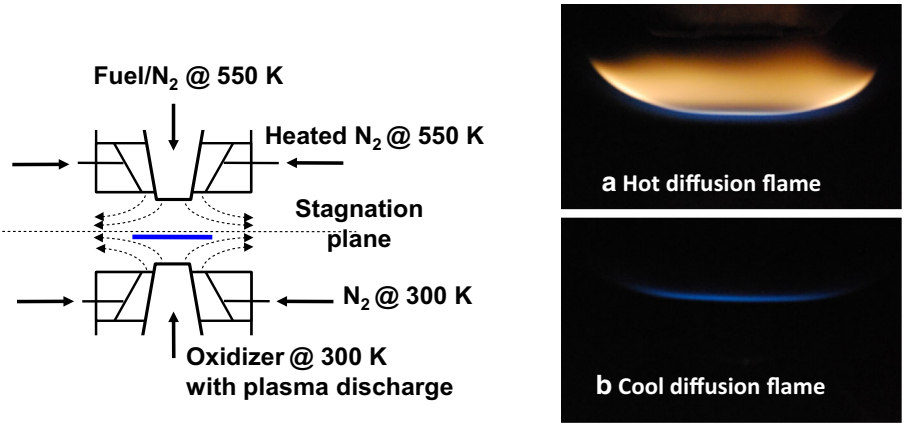

Fig. 8 *Left* Experimental setup of plasma assisted cool flame experiments. *Right* Direct images of *a* a normal hot diffusion flame (peak temperature: ~1900 K) and *b* a cool diffusion flame (peak temperature: ~650 K); pressure (1 atm) [19]

The measured and predicted temperature and species distributions of the cool diffusion flame by using thermocouples and micro gas chromatography (GC) are shown in Fig. 9a–c. The temperature measurements indicate that the cool diffusion flame has a maximum temperature of 640 K, which is much lower than that of the conventional high temperature diffusion flame (above 1600 K). Also, as seen in Fig. 9b, unlike the hot diffusion flames where the fuel is completely oxidized prior to the reaction zone, a large leakage of fuel (n-heptane) and oxygen across the cool diffusion flame is observed. Moreover, Fig. 9c shows that the cool diffusion flame partially oxidizes the fuel and produces significant amounts of H_2O, CO, and CH_2O [19]. Therefore, the observation of a cool diffusion flame at atmospheric pressure clearly demonstrates that plasma generated radicals (e.g. O) and intermediate species such as O_3 can significantly accelerate low temperature fuel oxidation. Without plasma generated O_3 chemical sensitization, cool flames were not able to be stabilized at such short flow residence time. Note that the competing reaction of $O + N_2 = NO + N$ has a very high activation energy and thus will not compete with reactions R1 and R2 at low temperature to consume active radicals.

Figure 10 shows the experimentally determined ignition and extinction diagram of cool diffusion flames with 4 % ozone addition in the oxidizer side. Three different flame regimes are shown in this figure: (1) the unstable cool flame, (2) the cool diffusion flame, and (3) the hot diffusion flame regimes. For example, at a flow strain rate of $a = 80\ s^{-1}$, there is no flame until the fuel concentration, X_f, reaches 0.085. From $0.085 < X_f < 0.105$, cool diffusion flames are formed from direct ignition via plasma generated ozone activation but are unstable, exhibiting repetitive ignition and extinction instability. Stable cool

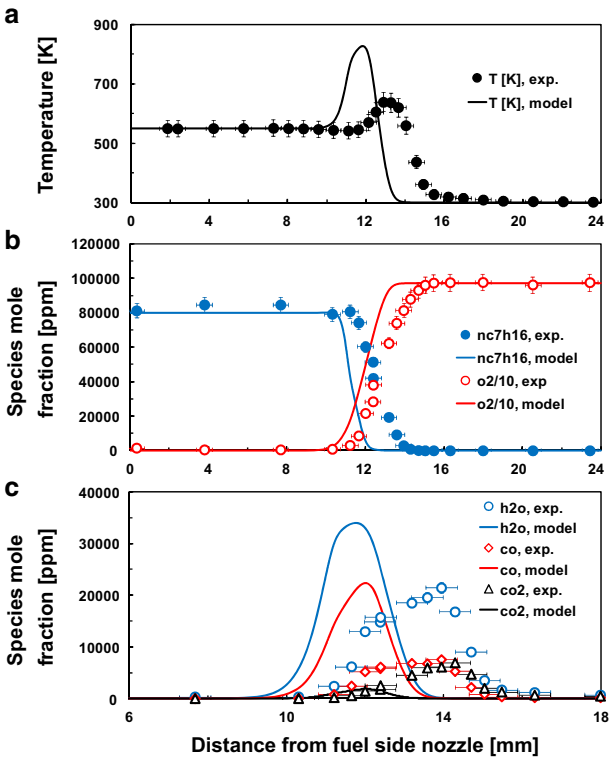

Fig. 9 Comparison of measured and computed temperature and major species distributions in the cool diffusion flame; pressure (1 atm) [19]

diffusion flames are observed from $0.105 < X_f < 0.125$. At higher fuel concentrations beyond $X_f > 0.125$, the direct initiation of hot diffusion flames is seen. Therefore, the existence of plasma assisted cool flame extends the lean ignition limit of the mixture. The ignition and extinction diagram without O_3 was also modeled and can be found in Ref. [19].

Plasma Assisted Premixed Cool Flames

Recently, experiments observing premixed cool flames at atmospheric pressure through ozone production by plasma were also conducted by using DME/oxygen mixtures in the same counterflow geometry [20, 25]. In this experiment, the fuel is premixed with oxygen and ozone at 300 K. A counter-flowing preheated nitrogen jet (600 K) is used to initiate the cool flame. The mole fraction of ozone produced by the plasma discharge in the oxygen stream remains between 3.1 and 3.4 %. The experiment shows that plasma generated ozone can also successfully initiate a premixed cool flame at atmospheric pressure.

A direct ICCD image of the plasma assisted premixed cool flame is shown in Fig. 11a. The measured and predicted cool flame regime diagram for premixed DME/O_2 mixtures with 3 % ozone is shown in Fig. 11b. Three distinct regions can be seen in this figure. At extremely low equivalence ratios, no stable flames can exist as the mixture is beyond the lean flammability limit for the cool flame. This lean limit slightly increases with increasing strain rate. At richer fuel concentrations, there exists a broad region of stable cool flames. Finally, when the equivalence ratio is increased further, the cool flame eventually destabilizes and transitions to a hot flame. The increased flame speed of the hot flame often results in a flame flashback. The present experiment clearly demonstrates that plasma assisted cool flames can significantly extend the lean burning limit of a fuel with low temperature chemistry. A significant further challenge to understanding the chemistry of cool flames is to quantitatively measure and predict the kinetic processes of plasma assisted low temperature combustion.

Kinetic Studies of Plasma Assisted Low Temperature Combustion

Low Temperature Oxidation of Methane in a Flow Reactor with Nanosecond Repetitively Pulsed Discharge

In order to understand the kinetic pathways of low temperature oxidation in plasma assisted combustion, experimental and numerical studies of low temperature methane

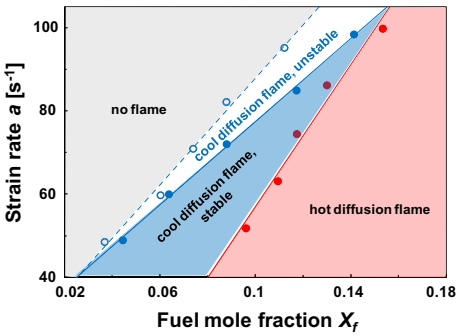

Fig. 10 Measured cool diffusion flame and hot diffusion flame ignition diagram as a function of fuel concentration X_f and flow strain rate a at 4 % ozone addition in the oxidizer stream; pressure (1 atm) [19]

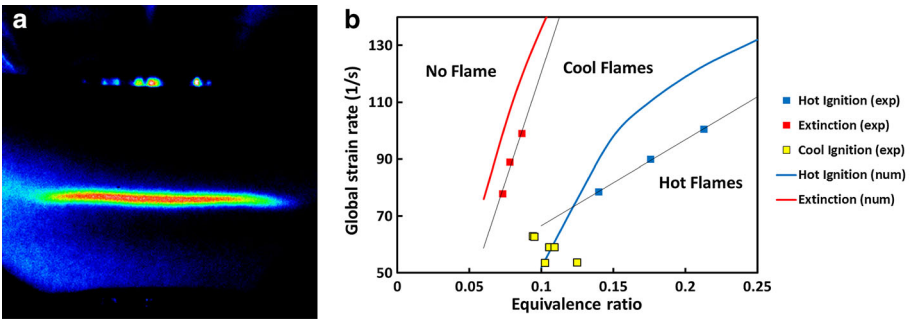

Fig. 11 **a** An image of the premixed DME/O_2/O_3 cool flame from an ICCD camera, **b** experimental and numerical results showing the cool flame regime diagram of a DME/O_2/O_3 premixture with 3 % ozone added in the counterflow configuration (at 1 atm)

oxidation in a nanosecond repetitively pulsed (NRP) discharge have been carried out [26, 27]. The experimental setup is shown in Fig. 12. The gas mixture used for all experiments is 0.083 CH_4, 0.167 O_2, and 0.75 He (stoichiometric, 75 % dilution), flowing at a velocity of 0.2 m/s and at a pressure of 60 Torr. A nanosecond pulse generator (FID GmbH FPG 30-50MC4) is used to generate the plasma, and the dielectric barrier discharge (DBD) consists of two 45 × 45 mm^2 stainless steel plates, separated by two sheets of quartz 1.6 mm thick and a 14 mm discharge gap. The pulse amplitude is maintained at 8.76 kV

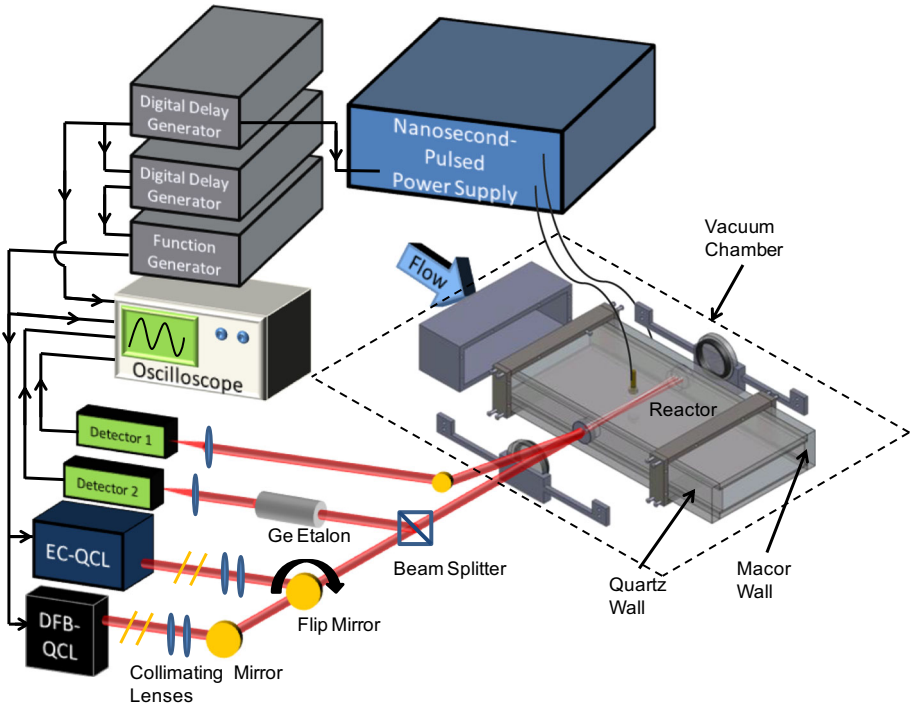

Fig. 12 Diagram of the experimental setup of the low temperature plasma reactor

for all experiments. Time dependent measurements are performed in a burst of 300 pulses and a pulse repetition frequency of 30 kHz, and continuously pulsed measurements are made at pulse frequencies in the range of 0.1–30 kHz. Per pulse energy deposition is measured to be 1.5 ± 0.2 mJ. The optical diagnostic systems consists of two mid-IR lasers, a continuous wave external cavity mode hop free (CW-EC-MHF) quantum cascade laser (QCL) from daylight solutions, and a distributed feedback (DFB) QCL from Alpes Lasers (sbcw3176). Temperature is measured using the daylight solutions laser by scanning two methane absorption lines at 1343.56 and 1343.63 cm^{-1}. The laser is scanned at a rate of 100 Hz, and the temperature profile is collected by the time difference between the plasma pulses and the laser scan. Time history measurements of formaldehyde are performed with the Alpes laser at 1726.79 cm^{-1}. In this case, the laser is scanned at a rate of 15,000 Hz. A miniature Herriott cell with 24 times beam reflections and 1.08 m optical path length is developed in the DBD reactor. A germanium etalon (FSR $\approx$ 0.74 GHz at 1345 cm^{-1}) is used to obtain the laser scan rate and quantify the wavelength. The detectors are MCT type (Vigo PVM-2TE10.6). The absorption profile is fitted using a Voigt profile and a least squares non-linear fitting algorithm, using HITRAN [28] line parameters and varying the concentration and pressure broadening parameters to obtain an optimized quantification. In addition to the laser absorption measurements, species quantification is also performed downstream of the plasma using gas chromatography (GC-TCD, Inficon 3000).

For kinetic modeling, we used a combination of ZDPlaskin [29] and SENKIN [30], which allows calculations of the electron collision reaction rates with the electron energy distribution function computed using BOLSIG+ [31] and chemical reactions using the adaptive time-stepping of CHEMKIN [26]. Energy transfer between molecules in ground states, electronically excited states and ions are also incorporated [32]. In addition, a heat loss term to account for conduction losses to the wall is added to the energy equation [33]. The low temperature kinetic model used here is a combination of the newly developed high pressure kinetic mechanism (HP-Mech) [34] and plasma reactions collected primarily from [35–38]. HP-Mech includes pressure dependence of reaction rates for all unimolecular reactions and can be applied from low pressure to high pressure conditions. Excited and ionized species such as $O_2(c^1\Sigma_u^-)$, $O_2(C^3\Delta_u)$, $O_2(A^3\Sigma_u^+)$, $O_2(a^1\Delta_g)$, $O_2\left(b^1\Sigma_g^+\right)$, O_2^+, $O(^1D)$, $O(^1S)$, O^+, $He(2s\ ^1S)$, CH_4^+, and CH_3^+ are included. Vibrationally excited species, negative ions and complex positive ions are neglected. The LXCat online database [39, 40] is used for electron-collision cross-sections. An update of the cross-sections for CH_4 is made by using the method described by Janev and Reiter [41]. A full reaction list can be found in [26].

The measured species concentrations by the GC-TCD sampling downstream of the plasma reactor are shown in Fig. 13. The predicted major species, including methane, oxygen, water, and carbon monoxide are all in good agreement with experimental data. This agreement indicates that the overall reaction rates for fuel consumption and oxidation are correct. However, for the intermediate species, the predicted concentrations of carbon dioxide and hydrogen are about a factor of two lower than the experimental data. Moreover, the concentration of formaldehyde is under-predicted by a factor of 4 and the methanol concentration is over-predicted by an order of magnitude, indicating that there is a large uncertainty in the low temperature plasma chemistry.

The time dependent measurement of formaldehyde is shown in Fig. 14. It is seen that the concentration is again under-predicted by a factor of four. To understand the reaction pathway of low temperature methane oxidation, Fig. 15 shows that reaction path flux

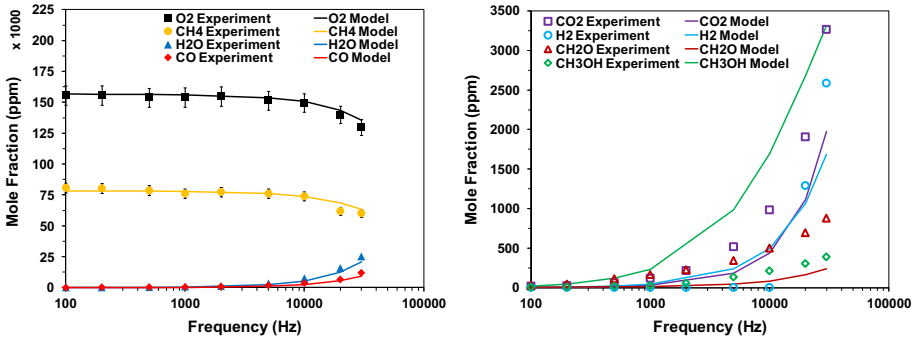

Fig. 13 Species measurements and modeling in a continuous plasma at 30 kHz repetition rate and 8.76 kV peak voltage in a stoichiometric CH_4/O_2/He mixture with 75 % dilution (pressure at 60 Torr) [26]

Fig. 14 Formaldehyde measurements and modeling during and after a 300 pulse burst at 30 kHz repetition rate and 8.76 kV peak voltage in a stoichiometric CH_4/O_2/He mixture with 75 % dilution (pressure at 60 Torr) [26]

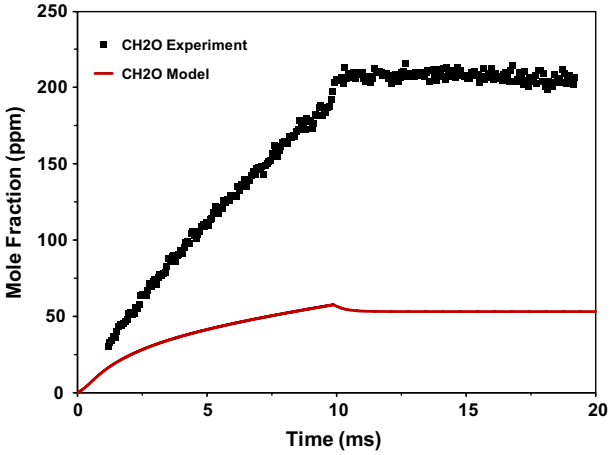

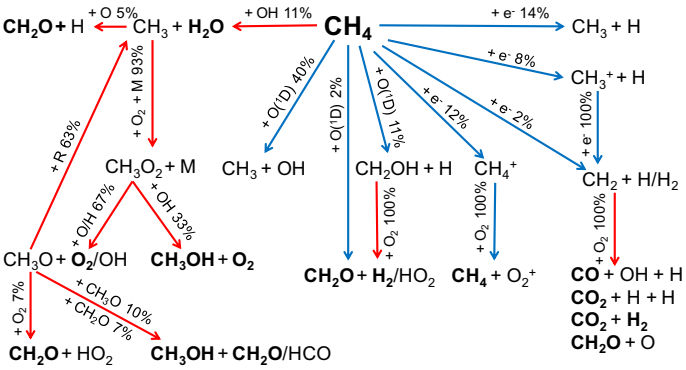

Fig. 15 Path flux for 30 kHz pulse repetition frequency at a steady state temperature of 407 K and pressure of 60 Torr

analysis for 30 kHz pulse repetition frequency at a steady state temperature of 407 K. The major fuel consumption pathways are through electron collision reactions and reaction with O(^{1}D). Particularly, the direct O(^{1}D) reaction with fuel is shown to be the major pathway to produce the initial OH and CH_3 radicals, which lead to the subsequent formation of formaldehyde and methanol. Note that the number density of excited He* is low due to its high excitation energy and has negligible impact on the kinetics at the experimental condition. Therefore, the large uncertainty in the prediction of formaldehyde and methanol may be attributed to the uncertainty of the rate constants and pathways of the O(^{1}D) reaction with fuel.

Low Temperature Oxidation of C_2H_4 in a Flow Reactor with Nanosecond Repetitively Pulsed Discharge

C_2H_4 is one of the major species of fuel pyrolysis and low temperature oxidation. Experiments and modeling of pyrolysis and low temperature oxidation of C_2H_4/Ar and C_2H_4/O_2/Ar mixtures in the DBD reactor are also carried out at a pressure of 60 Torr. Figure 16 shows the comparisons between model predictions and experimental results of the time-resolved concentrations of C_2H_2, CH_4, and H_2O formation. It is clear that HP-Mech [27, 34], which is developed particularly for low temperature and high pressure fuel oxidation based on direct experimental measurements and/or ab initio quantum chemistry calculations of the elementary reaction rate constants without global mechanism optimization, reproduces well the measured species time history with only slight under-prediction of C_2H_2. However, USC-Mech II [42] over-predicts H_2O formation by one order (Fig. 16b). The large discrepancy between the experiments and the USC-Mech II model predictions indicates that inclusion of low temperature fuel oxidation pathways in plasma assisted combustion is critical in reproducing the experimental data.

The path flux analysis of ethylene oxidation integrated over the first 10 ms after the initial plasma pulse is shown in Fig. 17. It is seen that there are three different major fuel consumption pathways. The first pathway is direct collisional dissociation by excited and ionized Ar (blue arrows) to form hydrocarbon fragments. The second pathway is fuel oxidation by plasma generated radicals such as O and O(^{1}D) (The red and green lines in Fig. 17). The last pathway is plasma activated low temperature oxidation involving O_2 addition to the fuel radicals, leading to $C_2H_5O_2$ (ethyl peroxy radical), $C_2H_5O_2H$ (ethyl

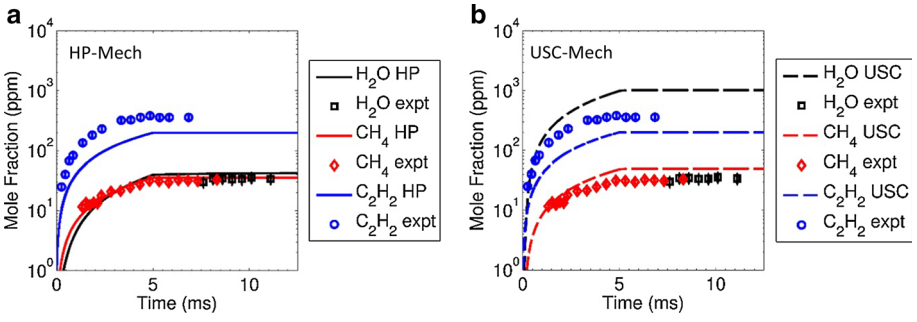

Fig. 16 Measurements and predictions of C_2H_2, CH_4, and H_2O concentrations after 150 pulses at 30 kHz repetition rate for a mixture of 6.25/18.75/75 C_2H_4/O_2/Ar by using **a** HP-Mech and **b** USC-Mech II (pressure of 60 Torr)

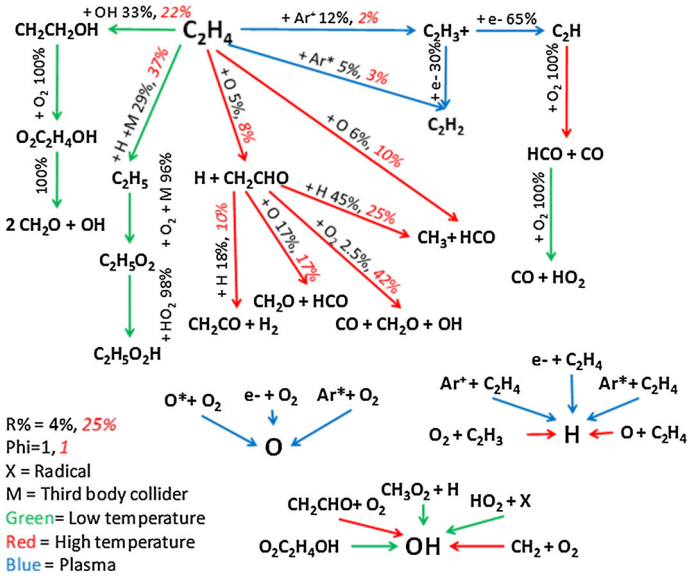

Fig. 17 Path flux analysis for plasma assisted low temperature C_2H_4 oxidation at 60 Torr

peroxide), or $O_2C_2H_4OH$ and subsequent decomposition into formaldehyde and hydroxyl radicals. Once again, Fig. 17 clearly shows that the inclusion of low temperature fuel oxidation pathways initiated by plasma generated radicals such as O, OH, and $O(^1D)$ in plasma assisted combustion is important to develop a predictive model.

Diluent has a great impact on plasma chemistry. The above plasma combustion kinetic mechanism was examined with Ar dilution. The kinetics for plasma assisted low temperature combustion with He dilution was investigated in [13] and [18], respectively, for methane and dimethyl ether. For reaction systems involving air without Ar and He dilutions, the mean electron energy will be higher and the electron number density is lower. Therefore, the reaction pathway involving electron impact dissociation and ionization may change. Moreover, radical production pathways via direct collisional dissociation by electronically and vibrationally excited nitrogen and oxygen molecules may become important [1–3, 12, 17, 33, 43]. In addition, for burst discharge, the electron energy distribution and the reaction rates during and between each pulse are different. Quantitative modeling of nano-second repetitive plasma assisted combustion needs to include pulse to pulse plasma activation process.

Studies of Low Temperature Fuel Oxidation Kinetics with $O(^1D)$ in a Photolysis Flow Reactor

$O(^1D)$ is one of the a few key electronic excited species in addition to singlet oxygen which have significant impact in low temperature fuel oxidation. Many previous experimental studies have been focused on oxygen singlet [17, 44] In order to understand low temperature reactions involving $O(^1D)$ with fuel, a photolysis flow reactor that combines mid-IR laser absorption and Faraday Rotation Spectroscopy (FRS) techniques is developed for accurate measurements of OH, HO_2, CH_2O, and other important intermediate species in the reactive flow system. The experimental setup is schematically shown in Fig. 18. The

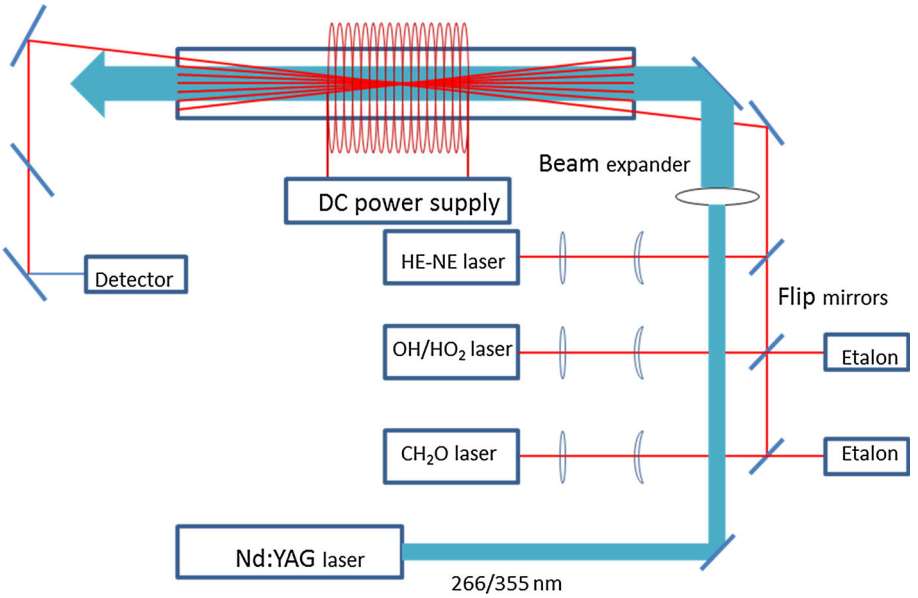

Fig. 18 Schematic illustration of the experimental setup of the Herriott type multi-pass cell photolysis flow reactor. The gas flow system is not shown here

photolysis reactor consists of a quartz reactor (913 mm in length) with a pair of spherical mirrors (500 mm focal length) installed at both ends of the reactor to form a multi-pass Herriott cell. The mirrors are made of UV-grade CaF_2 offering greater than 90 % transmission from UV to mid-IR (8 μm). The central portion of the concave side of the mirror (40 mm diameter) allows for transmission of the UV light for photolysis. The outside rim starting 8 mm from the edge of the mirror has a protected gold coating to form a reflective, multi-pass IR Herriot cell. The design provides a 655 mm geometric overlap between the IR and the photolysis UV laser beams (with a 40 mm diameter) in the center portion of the reactor for a single-pass. For FRS detection of HO_2 and OH, a 30 cm long and 6.35 cm diameter water-cooled solenoid coil is installed, providing an external magnetic field. The quadruple harmonic output (266 nm) of a pulsed Nd:YAG laser is expanded to 20 mm diameter (at current stage) into the flow reactor. The multi-pass cell with 21 passes provides a 19.17 total meter path length between the mirrors and an effective 6.17 meter absorption path length for species diagnostics (HO_2, OH, CH_2O and H_2O) given the geometric overlap with the 20 mm diameter UV photolysis laser beam.

The photolysis reactor is used in kinetic studies of $O_3/O_2/CH_3OH/Ar$ mixtures [45]. Ozone is generated by a plasma dielectric barrier discharge from oxygen (Ozone Solutions, TG-20) and is mixed with other species downstream. $O(^1D)$ is produced by the 266 nm laser photolysis of ozone in the flow reactor to initiate the reaction. Based on the photon-ionization cross-section (9×10^{-18} cm^2/mol), the laser photon flux (1.52×10^{17}), and ozone concentration (596 ppm), the estimated $O(^1D)$ concentration is about 2.16×10^{14} mol/cm^3 with 10 % uncertainty. Time-resolved CH_2O and H_2O profiles at 40 Torr have been obtained by direct absorption spectroscopy at 1726.8 and 1338.55 cm^{-1}, respectively.

Figure 19 shows the comparison of experimental measured time history of H_2O with simulation using HP-Mech with laser photolysis of 1.91 % O_2, 0.224 % CH_3OH, and 596 ppm of O_3 in Argon mixture. It is seen that HP-Mech under-predicts H_2O formation at early time but over predicts in later time [45]. The prompt H_2O formation measured experimentally shows very strong evidence of a missing pathway in the kinetic models involving direct reactions between $O(^1D)$ with CH_3OH. The total rate of $O(^1D)$ with CH_3OH have been measured a couple of times [46, 47]. However, there are large uncertainties on the product channel identification and quantification [46–48]. In original HP-Mech, only R27 and R28 are included since they are discussed both experimentally and theoretically [46, 48] and the branching ratio is set to be 0.55–0.45 as k_o shown below [45].

$$\begin{aligned} &O(^1D) + CH_3OH \rightarrow CH_2OH + OH \\ &k_o = 1.8 \times 10^{14}\left(\text{mol cm}^3\,\text{s}\right)\, k_{new} = 1.5 \times 10^{14}\left(\text{mol cm}^3\,\text{s}\right) \end{aligned} \tag{R27}$$

$$\begin{aligned} &O(^1D) + CH_3OH \rightarrow HOCHOH + H \\ &k_o = 1.2 \times 10^{14}\left(\text{mol cm}^3\,\text{s}\right)\, k_{new} = 0.5 \times 10^{14}\left(\text{mol cm}^3\,\text{s}\right) \end{aligned} \tag{R28}$$

$$O(^1D) + CH_3OH \rightarrow CH_2O + H_2O \quad k_o = 0\left(\text{mol cm}^3\,\text{s}\right)\, k_{new} = 1.0 \times 10^{14}\left(\text{mol cm}^3\,\text{s}\right) \tag{R29}$$

A theoretical prediction of the potential energy surface (PES) of $O(^1D) + CH_3OH$ is investigated at M062X/cc-pvtz level [45]. As shown in Fig. 20, the reaction channel R29 for the production of $CH_2O + H_2O$ is found to have the lowest barrier (~50 kcal/mol) compared with the other two reaction channels (R28 and R27). The significantly lower energy barrier for the radical termination $CH_2O + H_2O$ channel may provide a key pathway for the $O(^1D) + CH_3OH$ reaction to directly produce H_2O. This prompt H_2O formation pathway can explain the discrepancies of branching ratios between the two

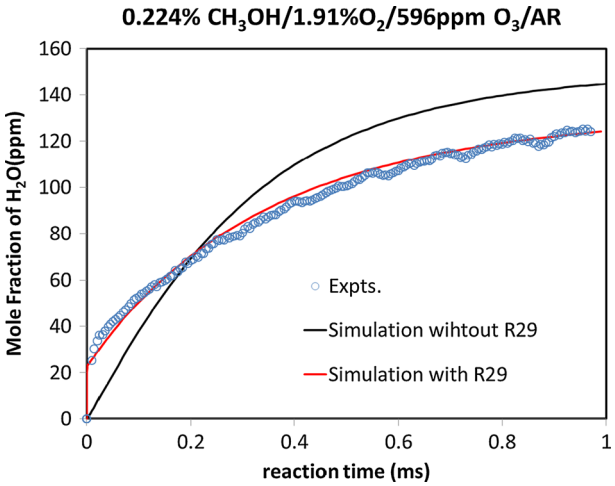

Fig. 19 Time-resolved mole fraction of H_2O in the 266 nm laser photolysis of 0.224 % CH_3OH 1.91 % O_2 and 596 ppm O_3 in Ar mixture with the variation of CH_3OH flow rate compared to model simulations for 1.0 ml/h flow of CH_3OH. *Circled curve* Experimental measurement. *Solid black curve* simulation using the original model. *Solid red curve* simulation with updated reaction rates (40 Torr) [45] (Color figure online)

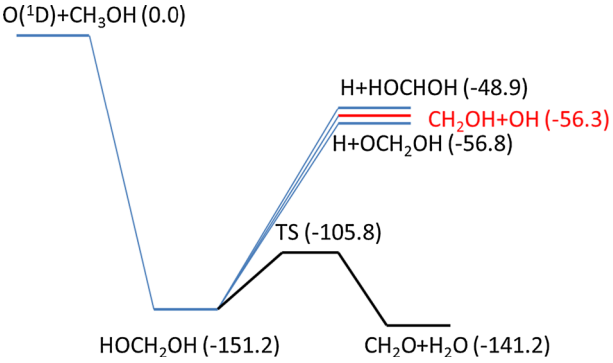

Fig. 20 Schematic of potential energy surfaces of $O(^1D) + CH_3OH$ at M062X/cc-pvtz level [45]. Energy unit: Kcal/mol

experimental measurements [46, 47] and also the current H_2O profile at early time shown in Fig. 19 with a set of k_{new} for R27, R28, and R29. However, in future research the accuracy of the PES needs to be improved, and the reaction rate constant needs to be accurately determined from the cross-validation of experimental results and high order quantum computation.

Note that practical combustion systems mostly operate at high pressure. Although at high pressure, the plasma properties and the reaction pathways of plasma assisted combustion may change significantly from that of low pressure, except few unimolecular reactions, most elementary rate constants validated in low pressure environments remain the same. Therefore, low pressure experiments can provide quantitative validation of elementary rate constants for some key reactions. However, it should be noted that due to the change of reaction pathways the mechanism needs to be validated against high pressure experiments before using it for modeling. As such, high pressure plasma assisted combustion experiments with well-defined boundary conditions are very critical for validated mechanism development for engine applications.

Conclusion

Non-equilibrium plasma has a significant kinetic enhancement effect on ignition and flame stabilization. The radical production process by electrons, ions, and electronically and vibrationally excited molecules in non-equilibrium plasma is faster than that of the key chain-branching processes of combustion particularly at low and intermediate temperature; thus, it can dramatically shorten the ignition delay time. The experimental results show that plasma can enhance low temperature combustion so greatly that it can lead to a direct ignition to flame transition without an extinction limit. Moreover, it is also demonstrated that radical production by plasma can enable self-sustained cool flame formation even at atmospheric pressure at a few millisecond timescale. Comparison between model predictions and in situ laser diagnostics show that plasma plays a critical role in producing active species, thus activating the fuel oxidation pathways even at low temperature, which cannot be accessed in conventional combustion mode. Although the updated HP-Mech/-plasma mechanism can reproduce the major species and products of plasma assisted combustion at low temperature, there remain major limitations in predicting intermediate

species via the low temperature plasma assisted pathways. Kinetic analysis shows that fuel oxidation by $O(^1D)$ plays an important role in producing the initial radicals at low temperature. However, there are large uncertainties in the rates of the $O(^1D)$ reaction with fuel. Particularly, the branching ratio between the chain-branching and chain-terminating reaction channels is not well known. The results suggest that there are missing reaction pathways in low temperature plasma assisted combustion which need to be addressed in future studies.

Acknowledgments This work is partly supported by AFOSR plasma MURI project, US Department of Energy, Office of Basic Energy Sciences as part of an Energy Frontier Research Center on Combustion with Grant No. DE-SC0001198, the NSF Grants of CMMI-1449314 and CBET-1507358, and the Open Fund of State Key Laboratory of High-temperature Gas dynamics, Institute of Mechanics, CAS with Grant No. 2014KF04.

References

1. Ju Y, Sun W (2015) Plasma assisted combustion: dynamics and chemistry. Prog Energy Combust Sci 48:21–83. doi:10.1016/j.pecs.2014.12.002
2. Starikovskiy A, Aleksandrov N (2013) Plasma assisted ignition and combustion. Prog Energy Combust Sci 39:61–110
3. Starikovskaia SM (2006) Plasma assisted ignition and combustion. J Phys D Appl Phys 39:R265–R299
4. Ombrello T, Ju Y, Fridman A (2008) Kinetic ignition enhancement of diffusion flames by nonequilibrium magnetic gliding arc plasma. AIAA J 46(10):2424–2433
5. Chen Z, Burke MP, Ju Y (2009) Effects of Lewis number and ignition energy on the determination of laminar flame speed using propagating spherical flames. Proc Combust Inst 32(1):1253–1260
6. Matalon M (1983) On flame stretch. Combust Sci Technol 31(3–4):169–181
7. Ganguly BN (2007) Hydrocarbon combustion enhancement by applied electric field and plasma kinetics. Plasma Phys Controlled Fusion 49:B239
8. Pilla G, Galley D, Lacoste DA, Lacas F, Veynante D, Laux CO (2006) Stabilization of a turbulent premixed flame using a nanosecond repetitively pulsed plasma. IEEE Trans Plasma Sci 34:2471–2477
9. Leonov SB, Kochetov IV, Napartovich AP, Sabel VA, Yarantsev DA (2011) Plasma-induced ethylene ignition and flame holding in confined supersonic air flow at low temperatures. IEEE Trans Plasma Sci 39:781–787
10. Michael JB, Dogariu A, Shneider MN, Miles RB (2010) Subcritical microwave coupling to femtosecond and picosecond laser ionization for localized, multipoint ignition of methane/air mixtures. J Appl Phys 108:093308
11. Uddi M, Jiang N, Mintusov E, Adamovich IV, Lempert WR (2009) Atomic oxygen measurements in air and air/fuel nanosecond pulse discharges by two photon laser induced fluorescence. Proc Combust Inst 32:929–936
12. Stancu GD, Kaddouri F, Lacoste DA, Laux CO (2010) Atmospheric pressure plasma diagnostics by OES, CRDS and TALIF. J Phys D Appl Phys 43:124002
13. Sun W, Won SH, Ombrello T, Carter C, Ju Y (2013) Direct ignition and S-curve transition by in situ nano-second pulsed discharge in methane/oxygen/helium counterflow flame. Proc Combust Inst 34(1):847–855
14. Rusterholtz DL, Lacoste DA, Stancu GD, Pai DZ, Laux CO (2013) Ultrafast heating and oxygen dissociation in atmospheric pressure air by nanosecond repetitively pulsed discharges. J Phys D Appl Phys 46(46):464010
15. Kim W, Godfrey M, Cappelli M (2010) The role of in situ reforming in plasma enhanced ultra lean premixed methane/air flames. Combust Flame 157:374e83
16. Kosarev IN, Aleksandrov NL, Kindysheva SV, Starikovskaia SM, Starikovskii AY (2009) Kinetics of ignition of saturated hydrocarbons by nonequilibrium plasma: C2H6- to C5H12-containing mixtures. Combust Flame 156:221e33
17. Popov NA (2011) Effect of singlet oxygen O_2 ($a\ ^1\Delta_g$) molecules produced in a gas discharge plasma on the ignition of hydrogen–oxygen mixtures. Plasma Sources Sci Technol 20(4):045002
18. Sun W, Won SH, Ju Y (2014) In situ plasma activated low temperature chemistry and the S-curve transition in DME/oxygen/helium mixture. Combust Flame 161(8):2054–2063

19. Won SH, Jiang B, Diévart P, Sohn CH, Ju Y (2015) Self-sustaining n-heptane cool diffusion flames activated by ozone. Proc Combust Inst 35(1):881–888
20. Reuter C, Won SH, Ju Y (2015) Cool flames activated by ozone addition. In: 53rd AIAA aerospace sciences meeting. doi:10.2514/6.2015-1387
21. Filimonova EA (2015) Discharge effect on the negative temperature coefficient behaviour and multi-stage ignition in C_3H_8-air mixture. J Phys D Appl Phys 48(1):015201
22. Lefkowitz JK, Guo P, Ombrello T, Won SH, Stevens CA, Hoke JL et al (2015) Schlieren imaging and pulsed detonation engine testing of ignition by a nanosecond repetitively pulsed discharge. Combust Flame 162(6):2496–2507
23. Curran HJ, Gaffuri P, Pitz WJ, Westbrook CK (2002) A comprehensive modeling study of iso-octane oxidation. Combust Flame 129(3):253–280
24. Williams FA (1985) Combustion theory, 2nd edn. The Benjamin/Cummings Publishing Company, Menlo Park
25. Ju Y, Reuter CB, Won SH (2015) Numerical simulations of premixed cool flames of dimethyl ether/oxygen mixtures. Combust Flame 162(10):3580–3588
26. Lefkowitz JK, Guo P, Rousso A, Ju Y (2015) Phil Trans R Soc A 373(2048):20140333
27. Lefkowitz JK, Uddi M, Windom BC, Lou G, Ju Y (2015) In situ species diagnostics and kinetic study of plasma activated ethylene dissociation and oxidation in a low temperature flow reactor. Proc Combust Inst 35(3):3505–3512
28. Rothman LS, Gordon IE, Barbe A et al (2009) J Quant Spectrosc Ra 110(9–10):533–572
29. Pancheshnyi S, Eismann B, Hagelaar GJM, Pitchford LC (2008) University of Toulouse, LAPLACE, CNRS-UPS-INP, Toulouse, France. http://www.zdplaskin.laplace.univ-tlse.fr
30. Lutz AE, Kee RJ, Miller JA (1988) Sandia National Laboratories Report SAND87-8248
31. Hagelaar GJM, Pitchford LC (2005) Plasma Sources Sci Technol 14(4):722–733
32. Flitti A, Pancheshnyi S (2009) Eur Phys J Appl Phys 45(2):21001
33. Adamovich IV, Li T, Lempert WR (2015) Kinetic mechanism of molecular energy transfer and chemical reactions in low-temperature air-fuel plasmas. Philos Trans A Math Phys Eng Sci 373(2048). doi:10.1098/rsta.2014.0336
34. Yang X, Shen X, Santner J, Klippenstein SJ, Ju Y (2015) A high pressure mechanism (HP-Mech) for flame modeling of C_0–C_2 hydrocarbons, alcohols and methyl esters. The 9th US National Meeting on Combustion, Cincinnati
35. Sun W, Uddi M, Won SH, Ombrello T, Carter C, Ju Y (2012) Combust Flame 159(1):221–229
36. Capitelli M, Ferreira CM, Osipov AI, Gordiets BF (2000) Plasma kinetics in atmospheric gases. Springer, Berlin
37. Stafford DS, Kushner MJ (2004) J Appl Phys 96(5):2451
38. Kosarev IN, Aleksandrov NL, Kindysheva SV, Starikovskaia SM, Starikovskii AY (2008) Combust Flame 154(3):569–586
39. Phelps database. www.lxcat.net. Retrieved 4 Oct 2014
40. Biagi-v7.1 database. www.lxcat.net. Retrieved 4 Oct 2014
41. Janev RK, Reiter D (2002) Phys Plasmas 9:4071
42. Wang H, You X, Joshi AV, Davis SG, Laskin A, Egolfopoulos F, Law CK. http://ignis.usc.edu/USC_Mech_II.htm
43. Adamovich IV, Lempert WR (2015) Challenges in understanding and predictive model development of plasma-assisted combustion. Plasma Phys Controlled Fusion 57(1):014001
44. Ombrello T, Won SH, Ju Y, Williams S (2010) Flame propagation enhancement by plasma excitation of oxygen. Part II: effects of O_2 ($a^1\Delta_g$). Combust Flame 157(10):1916–1928
45. Yang X, Lefkowitz JK, Brumfield BE, Chen Q, Wysocki G, Ju Y (2015) Kinetics studies of O_3/O_2/CH_3OH/Ar mixtures in a photolysis flow reactor. The 9th US National Meeting on Combustion, Cincinnati
46. Matsumi Y, Inagaki Y, Kawasaki M (1994) Isotopic branching ratios and translational energy release of H and D atoms in the reaction of $O(^1D)$ with CH_3OD and CD_3OH. J Phys Chem 98:3777–3781
47. Osif TL, Simonaitis R, Heicklen J (1975) The reactions of $O(^1D)$ and HO with CH_3OH. J Photochem 4:233–240
48. Huang CK, Xu ZF, Nakajima M, Nguyen HMT, Lin MC, Tsuchiya S, Lee YP (2012) Dynamics of the reactions of $O(^1D)$ with CD_3OH and CH_3OD studied with time-resolved Fourier-transform IR spectroscopy. J Chem Phys 137:164307